Modification of the Crystalline Structure of ZnO Nanoparticles Embedded Within a SiO$_2$ Matrix due to Thermal Stress Effects

Alejandra Garcia-Sotelo^a, Mario Avila-Meza^b, Miguel Angel Melendez-Lira^a* [ORCID]*, *Jose Luis*

Fernandez-Muñoz^c, Orlando Zelaya-Angel^a

^{a}*Departamento de Física, Centro de Investigación y de Estudios Avanzados del IPN, Ciudad de México, México*
^{b}*Maestría en Ciencias e Ingeniería de Materiales, Universidad Autónoma Metropolitana campus Azcapotzalco, Ciudad de México, México*
^{c}*Centro de Investigación en Ciencia Aplicada y Tecnología Avanzada, Instituto Politécnico Nacional, Ciudad de México, México*

Self-assembled nanocrystals of ZnO were embedded within a SiO$_2$ matrix by a sequential deposit using reactive R.F. sputtering. The ZnO nanoparticles (NP's) were obtained by depositing a very thin layer (~20 nm) of Zn on the bottom of the valleys of a first SiO$_2$ rough surface and then covered by another SiO$_2$ layer at 500 °C. The stress produced, due to the cooling process, by the SiO$_2$ matrix on the ZnO NP's generates an unusual crystalline phase of ZnO. The crystal structure was determined by means of X ray diffraction patterns. The ZnO + SiO$_2$ composite shows a transmittance higher than 80 % for wavelengths > 450 nm. Optical absorption allows to reveal the character and value of the optical band gap. Vibrational modes of the material were determined by Raman spectroscopy.

Keywords: *II-VI Semiconductor nanoparticles, reactive R.F. sputtering, Raman spectroscopy, thermal expansion coefficient.*

1. Introduction

Among transparent semiconductors ZnO has a relevant role because its intrinsic properties as a bulk material and the facility to produce both as thin film or nanostructures. The preparation of ZnO films include the whole list of available techniques: Sol-gel, spray pyrolysis, sputtering, laser ablation, molecular beam epitaxy, etc. [1-5]. Similarly there are many reports on the synthesis of ZnO nanostructures employing the most diverse methodologies ranging from chemical, vapor phase, electrochemical, etc. [6-9]. The direct band gap value of ZnO (3.4 eV), its large exciton binding energy (60 meV) and structural properties foster applications in diverse fields between them UV detection, enhancement of photovoltaics performance, photocatalysis, etc [10-13]. The control of the dispersion and distribution of the size of the nanoparticles employing simple fabrication techniques is a difficult task. Also, ZnO nanoparticles, produced by chemical methods, frequently have residues that would affect negatively its performance. In this work it is reported an effect observed when reactive RF sputtering is employed to deposit SiO$_2$/metallic Zn/SiO$_2$ on quartz and p-type silicon substrates; the valleys in the first rough SiO$_2$ layer acted as nucleation centers to the formation of self-assembled ZnO nanoparticles produced due to the oxidation process associated with the reactive atmosphere [14]. Samples are characterized by X-ray diffraction, electron transmission microscopy, UV-Vis and Raman spectroscopies.

The results confirm the formation of ZnO nanoparticles embedded in a SiO$_2$ matrix. ZnO nanocrystals with an unusual crystalline phase are found. This unusual phase is formed due a tensile stress effect on the ZnO nanoparticles produced by the lower thermal expansion coefficient of the SiO$_2$ matrix.

2. Material and Methods

Reactive sputtering of a silicon target 99.999% of purity was carried out in an O$_2$+Ar plasma to grow SiO$_2$ films on Si-111 and quartz substrates at 500 °C. The base pressure in the chamber was better than 1x10^{-6} Torr. A ratio of O$_2$ to Ar of 0.5, maintaining the total gas pressure at 15 mTorr, was employed for the working atmosphere. The R.F. power applied on the Si target was 100 W. The SiO$_2$ /Zn/ SiO$_2$ heterolayers were grown as follows: initially a layer of SiO$_2$ was deposited, then a thin layer of Zn, and finally a SiO$_2$ layer (see Fig. 1). The plasma was turned off and the chamber evacuated after the deposition of each layer. The Zn layer was grown by sputtering a metallic Zn target 99.999% of purity under an Ar pressure of 15 mTorr applying a rf power of 15 W. ZnO nanoparticles grown due to the interaction of the Zn thin layer with the reactive atmosphere. The topography of the samples was evaluated by atomic force microscopy, employing an Autoprobe CP Research 7 microscope in contact mode. The structural properties of the samples were obtained by grazing angle X-ray diffraction (XRD) of the CuK_α wavelength in a Siemens D5000 system.

*e-mail: mlira@fis.cinvestav.mx

Nanostructure characteristics were obtained by transmission electron microscopy (TEM) studies using a JEOL JEM-2010 electron microscopy at 200 KV. Film flakes were obtained scrapping the samples with a scalpel. UV-Vis spectroscopy was done in a Perkin-Elmer equipment. Room temperature Raman spectroscopy was carried out in a Horiba Jobin Yvon LabRAM micro-Raman system equipped with the 488 nm line of an Ar^+ laser.
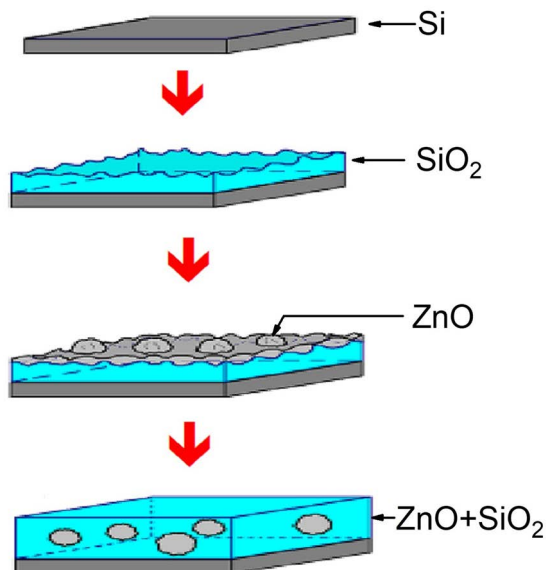

Figure 1. ZnO nanoparticles are formed through the oxidation of metallic Zn accumulated within the SiO_2 valleys.

3. Results and Discussion

The process to obtain the ZnO nanoparticles (NP's) embedded in a SiO_2 matrix is illustrated in Fig. 1. A Zn thin layer is deposited on the surface of a first SiO_2 layer grown on the Si substrate. The Si oxide film has a rough surface as observed in Fig. 2. The thin zinc layer covers completely the SiO_2 surface, once the reactive process is activated to deposit the top SiO_2 layer, the Zn layer on the crests reacts immediately and is etched away. So, it is plausible to expect the presence of some ZnO dispersed within the SiO_2 matrix. The formation of ZnO nanoparticles is promoted within the valleys of the rough SiO_2 surface. Valleys act as nucleation centers promoting the formation of ZnO nanocrystals while Zn reacts with oxygen them act like Zn containers. At the end of the process ZnO nanocrystals embedded in a SiO_2 matrix are obtained. As the roughness of the SiO_2 can be controlled through the parameters of the deposition process this methodology is an alternative to control ZnO nanoparticle size and, because the characteristics of the reactive atmosphere, to control oxygen vacancies in ZnO [15].

By means of the Scherrer formula it is found that under the conditions employed in this work ZnO NP's with average size of 8 ± 2 nm were obtained. To carry out TEM characterization a film flake was peeled off from the sample. A section of the TEM image of the ZnO-SiO_2 system is displayed in Fig. 3, where a ZnO NP of about 5 ± 1 nm can be appreciated immersed within amorphous SiO_2 [16]. A grazing angle XRD pattern (red) obtained from the same sample is exhibited in Fig. 4 along with the XRD powder patterns of the four different crystalline phases of ZnO reported in the literature: (*a*) cubic ZB [17] and RS [18] (*b*) hexagonal WZ (JCPDS 4-831), (*c*) unclassified (JCPDS 21-1486). An analysis of Fig. 4 indicates that the NP's can be constituted of the four reported different crystalline phases of ZnO, that is, these phases WZ, ZB, and RS cannot be discarded at all. Slight displacements of the interplanar spacing can be also expected because the pressure associated with the different values in thermal expansion coefficient of ZnO and SiO_2[19, 20]. The unclassified crystalline phase seems to be the principal structure with preferred orientation along the direction indicated by the $2\theta \approx 39°$ reflection. Rykl and Bauer [21] reported for first time a crystalline phase of ZnO different to the hexagonal and cubic, which, to our best knowledge, its crystal symmetry remains unidentified. That ZnO phase has also been marginally reported by other authors: in N doped thin films [22], in porous hollow microspheres [23] and oxidation of Langmuir–Blodgett multilayers [24]. This phase was obtained by Rykl and Bauer at high temperatures (450 °C) and high pressures (600 atm) [21]. The high growth temperature and/or stress induced by doping have been probably the cause of the crystalline change in the aforementioned reports. In our case, the more probable origin of that unusual phase is the tensile stress produced by the SiO_2 matrix. As the sample gets cooled down to room temperature the lower thermal expansion coefficient of SiO_2 avoids that ZnO attains its freestanding crystalline characteristics causing the presence of stress.
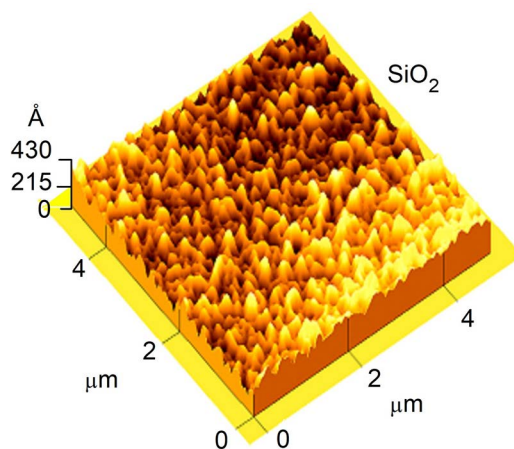

Figure 2. Texture of the first SiO_2 layer deposited by reactive RF sputtering obtained by AFM microscopy.
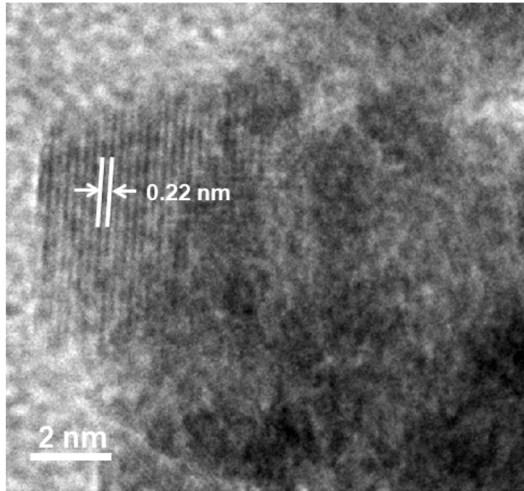
Figure 3. Transmission electron micrograph of a ZnO nanoparticle. Crystalline planes are shown.
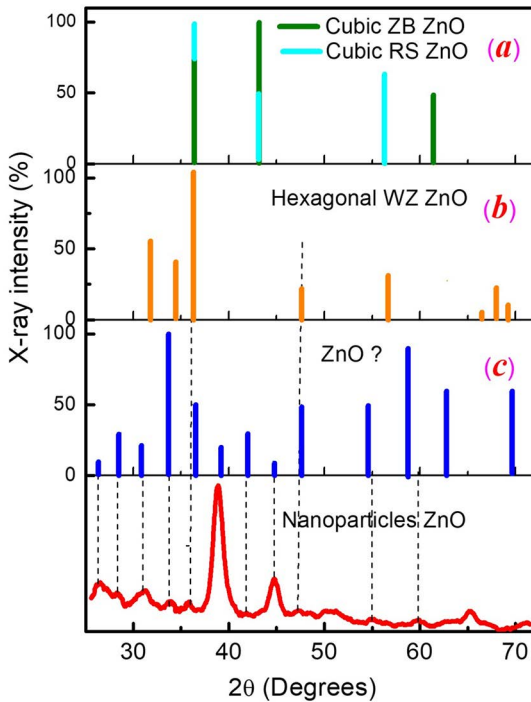

Figure 4. At the bottom it is shown the experimental X-ray diffractogram (a) X-ray diffractograms of cubic (b) hexagonal and (c) unknown ZnO crystal structures.

The optical transmittance of a sample deposited on quartz substrate is shown in the inset (*a*) of Fig. 5. The aspect of the experimental data-line suggests the presence of two optical band gaps (E_g's). Actually, the potential presence of several crystalline phases does not allow the unambiguously determination of the band gaps. However, to afford more information about the electronic properties of the unknown ZnO phase a possible assignation is proposed. The insets (*b*) and (*c*) in Fig. 5 present the application of the Tauc's method for the determination of direct and indirect band gap values.
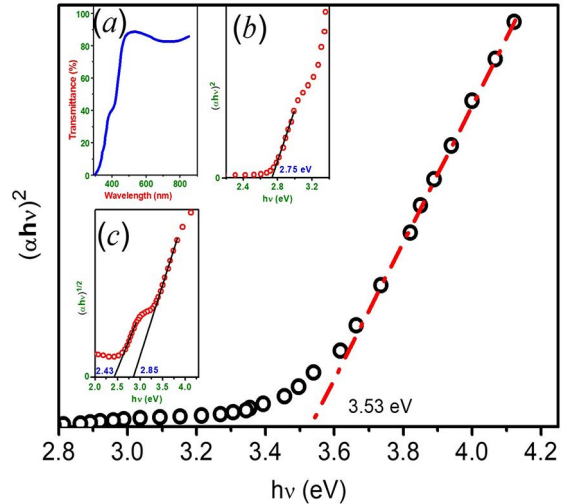

Figure 5. Tauc's analysis of the transmission spectrum, inset (a), taking in account the possibility of a phase mixture. The graph corresponds to the Zinc Blend and/or Wurzite ZnO. Inset (b) Shows the possibility of a direct band gap associated with the unkown phase while inset (c) will show the presence of two indirect band gaps, from the RS and the unknown ZnO phases.

Segura et al. have reported that E_g of RS-ZnO has a value of 2.45 ± 0.15 eV [25]. An indirect $E_g = 2.43 \pm 0.05$ eV is obtained in the inset (*c*) of Fig. 5, which could be the E_g value of the RS-ZnO phase present in our system. The larger direct $E_g = 3.53 \pm 0.05$ eV could belong to E_g of NP's of WZ-ZnO /or ZB-ZnO [17]. Consequently, a good possibility exists that unknown phase have indirect and direct E_g values of 2.75 and 2.85 eV, respectively. A contribution to the absorption from the matrix is impossible as for SiO_2 $E_g \cong 9$ eV [26]. Raman characterization was carried out on both samples, grown on Si and quartz substrates. The Raman spectra taken on the sample grown on silicon was dominated by the silicon phonon distribution avoiding obtaining any information. The Raman spectrum of the sample grown on quartz is displayed in Fig. 6.
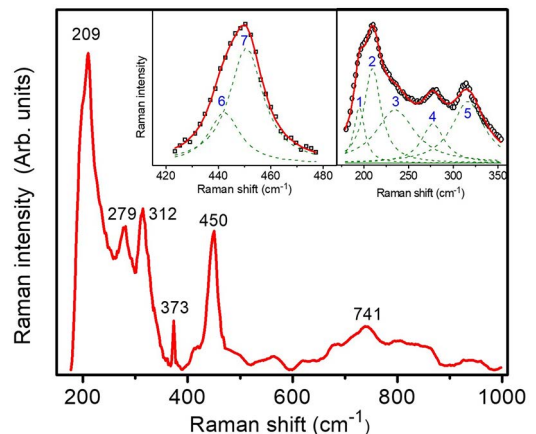

Figure 6. Room temperature Raman spectrum. The insets shown possible contributions from the unknown ZnO phase.

According to Zhao et al [22], the mode around 440 cm^{-1} corresponds specifically to that of the unknown crystalline phase, which appears in the left inset of Fig. 6, in the deconvolution of the mode at 450 cm^{-1}, at around 440 cm^{-1}. The modes shown in the Raman spectrum in Fig. 6 (see also right inset) different to those reported in the literature for ZnO [27-30], at normal and under high pressure conditions, are these located at 190, 233, 318, and 741 cm^{-1}. It is possible that low frequencies modes are associated with the unknown crystalline phase of ZnO.

4. Conclusions

By means of R.F. sputtering ZnO nanoparticles embedded within a SiO_2 matrix were synthesized and deposited on Si and quartz substrates. The tensile stress on ZnO NPs due to the SiO_2 matrix surrounding them induced a transition of phase producing the reported unidentified crystalline phase of ZnO. This phase has been obtained in the past under high pressures and high temperatures mostly using methods adequate to produce volumetric samples. The use of thermal expansion properties as a control parameter to obtain this phase of ZnO could be a useful tool to obtain reproducible thin films. The characterization by UV-Vis transmittance and Raman spectroscopies allow us to propose possible values of the direct and indirect optical band gaps and vibrational modes for this unknown phase.

5. Acknowledgements

6. References

1. Fujihara S, Kusakado J, Kimura T. Fluorine Doping in Transparent Conductive ZnO Thin Films by a Sol-gel Method Using Trifluoroacetic Acid. *Journal of Materials Science Letters*. 1998;17(9):781-783.

2. Guillén-Santiago A, de la L Olvera M, Maldonado A, Asomoza R, Acosta DR. Electrical, structural and morphological properties of chemically sprayed F-doped ZnO films: effect of the ageing-time of the starting solution, solvent and substrate temperature. *Physica Status Solid (a)*. 2004;201(5):952-959.

3. Mosquera AA, Horwat D, Rashkovskiy A, Kovalev A, Miska P, Wainstein D, et al. Exciton and core-level electron confinement effects in transparent ZnO thin films. *Scientific Reports*. 2013;3:1714.

4. Gluba MA, Nickel NH, Hinrichs K, Rappich J. Improved passivation of the ZnO/Si interface by pulsed laser deposition. *Journal of Applied Physics*. 2013;113(4):043502.

5. Ko HJ, Chen Y, Hong SK, Yao T. MBE growth of high-quality ZnO films on epi-GaN. *Journal of Crystal Growth*. 2000;209(4):816-821.

6. Renaud A, Cario L, Rocquelfelte X, Deniard P, Gautron E, Faulques E, et al. Unravelling the origin of the giant Zn deficiency in wurtzite type ZnO nanoparticles. *Scientific Reports*. 2015;5:12914.

7. Ma JG, Liu YC, Xu CS, Liu YX, Shao CL, Xu HY, et al. Preparation and characterization of ZnO particles embedded in SiO_2 matrix by reactive magnetron sputtering. *Journal of Applied Physics*. 2005;97(10):103509.

8. Skompska M, Zarębska K. Electrodeposition of ZnO Nanorod Arrays on Transparent Conducting Substrates–a Review. *Electrochimica Acta*. 2014;127:467-488.

9. Borse RY. Characterization of thick solid films of Nano ZnO prepared by Self-propagating Solution Combustion Method. *Bionano Frontier*. 2015;8:73-76.

10. Krishnamoorthy S, Iliadis AA. Development of high frequency ZnO/SiO_2/Si Love mode surface acoustic wave devices. *Solid-State Electronics*. 2006;50(6):1113-1118.

11. Gogurla N, Sinha AK, Santra S, Manna S, Ray SK. Multifunctional Au-ZnO Plasmonic Nanostructures for Enhanced UV Photodetector and Room Temperature NO Sensing Devices. *Scientific Reports*. 2014;4:6483.

12. MacDonald BI, Della Gaspera E, Watkins SE, Mulvaney P, Jasieniak JJ. Enhanced photovoltaic performance of nanocrystalline CdTe/ZnO solar cells using sol-gel ZnO and positive bias treatment. *Journal of Applied Physics*. 2014;115(18):184501.

13. Zhang X, Shao C, Zhang Z, Li J, Zhang P, Zhang M, et al. In situ Generation of Well-Dispersed ZnO Quantum Dots on Electrospun Silica Nanotubes With High Photocatalytic Activity. *ACS Applied Materials Interfaces*. 2012;4(2):785-790.

14. Avila-Meza MF, Zelaya-Angel O, Gallardo S, Fernández-Muñoz JL, Alfaro-Flores DR, Meléndez-Lira MA. Synthesis and Characterization of Self-Assembled ZnO Nanoparticles Embedded Within a SiO_2 Matrix Deposited on (111) *p*-Type Silicon By Reactive RF Sputtering Using Metallic Zinc Target As Precursor. *Journal of Electronic Materials*. 2018;47(11):6607-6612.

15. Thornton JA. The microstructure of sputter-deposited coatings. *Journal of Vacuum Science & Technology A*. 1986;4(6):3059-3065.

16. Wu WF, Chiou BS. Properties of radio frequency magnetron sputtered silicon dioxide films. *Applied Surface Science*. 1996;99(3):237-243.

17. Martínez-Pérez L, Muñoz-Aguirre N, Muñoz-Aguirre S, Zelaya-Angel O. Nanometric structures of highly oriented zinc blende ZnO thin films. *Materials Letters*. 2015;139:63-65.

18. Sokolov PS, Baranov AN, Dobrokhotov ZV, Solozhenko VL. Synthesis and thermal stability of cubic ZnO in the salt nanocomposites. *Russian Chemical Bulletin*. 2010;59(2):325-328.

19. Seko A, Oba F, Kuwabara A, Tanaka I. Pressure-induced phase transition in ZnO and ZnO− MgO pseudobinary system: A first-principles lattice dynamics study. *Physical Review B*. 2005;72(2):024107.

20. Tada H, Kumpel AE, Lathrop RE, Slanina JB, Nieva P, Zavracky P, et al. Thermal expansion coefficient of polycrystalline silicon and silicon dioxide thin films at high temperatures. *Journal of Applied Physics*. 2000;87(9):4189-4193.

21. Rykl D, Bauer J. Hydrothermalsynthese von Zinkit. *Kristall und Technik*. 1968;3(3):375-374.

22. Zhao Y, Li Z, Lv Z, Liang X, Min J, Wang L, et al. A new phase and optical properties of the N-doped ZnO film. *Materials Research Bulletin*. 2010;45(9):1046-1050.

23. Fang Y, Xia Z, Yu F, Sha J, Wang Y, Zhou W. Formation mechanism of hollow microspheres consisting of ZnO nanosheets. *CrystEngComm*. 2012;14(24):8615-8619.

24. Parhizkar M, Kumar N, Nayak PK, Singh S, Talwar SS, Major SS, et al. Nanocrystalline ZnO films prepared by pyrolysis of Zn-arachidate LB multilayers. *Colloids and Surfaces A: Physicochemical and Engineering Aspects*. 2005;257-258:445-449.

25. Segura A, Sans JA, Manjón FJ, Muñoz A, Herrera-Cabrera MJ. Optical properties and electronic structure of rock-salt ZnO under pressure. *Applied Physics Letters*. 2003;83(2):278-280.

26. Fujimura N, Ohta A, Makihara K, Miyazaki S. Evaluation of valence band top and electron affinity of SiO₂ and Si-based semiconductors using X-ray photoelectron spectroscopy. *Japanese Journal of Applied Physics*. 2016;55(8S2):08PC06.

27. Vinogradov EA, Mel'nik NN, Tsurkan AE, Kicherman LV. Raman spectra of ZnO single crystals. *Journal of Applied Spectroscopy*. 1997;26(6):764-767.

28. Calzolari A, Nardelli MB. Dielectric properties and Raman spectra of ZnO from a first principles finite-differences/finite-fields approach. *Scientific Reports*. 2013;3:2999.

29. Manjón FJ, Syassen K, Lauck R. Effect of Pressure on Phonon Modes in Wurtzite Zinc Oxide. *High Pressure Research*. 2002;22(2):299-304.

30. Decremps F, Pellicer-Porres J, Saitta AM, Chervin JC, Polian A. High-pressure Raman spectroscopy study of wurtzite ZnO. *Physical Review B*. 2002;65(9):092101.